Springer

Journal of Mechanical Science and Technology 23 (2009) 856~867

Journal of Mechanical Science and Technology

www.springerlink.com/content/1738-494x
DOI 10.1007/s12206-009-0207-9

The effect of nonequilibrium condensation on hysteresis phenomenon of under-expanded jets †

Heuy-Dong Kim[1,*], Min-Sung Kang[1], Yumiko Otobe[2] and Toshiaki Setoguchi[3]

[1]*School of Mechanical Engineering, Andong National University, Andong, 760-749, Korea*
[2]*Kitakyushu National College of Technology, Kitakyushu, 802-0985, Japan*
[3]*Department of Mechanical Engineering, Saga University, Saga, 840-8502, Japan*

(Manuscript Received October 1, 2008; Revised January 7, 2009; Accepted February 9, 2009)

Abstract

Under-expanded jets which are discharged from an orifice or a nozzle have long been subject of researches for aeronautical and mechanical applications. Provided that the jet pressure ratio and nozzle configuration are known, the major features of the steady jet are now well known. However, the jet pressure ratio is often varied even during the process in many practical applications. Many questions remain unanswered with regard to how the supersonic jet responds to the transient process of the pressure ratio and whether the steady jet data for a specific pressure ratio can still bear the same during the transient process of pressure ratio. In the present study, the hysteric phenomenon of under-expanded jets has been investigated with the help of computational fluid dynamics methods. The under-expanded jets of both dry and moist air have been employed to investigate the transient processes of the pressure ratio. The effects of nonequilibrium condensation occurring in the under-expanded moist air jets are explored on the hysteresis phenomenon. It is known that under-expanded air jet produced during the startup transient of jet behaves differently from the shutdown transient process, leading to the hysteric phenomenon of under-expanded jet. It is also known that the moist air jet reduces the hysteric phenomenon, compared with the dry air jet, and that non-equilibrium condensation which occurs in the under-expanded moist air jet is responsible for these findings.

Keywords: Compressible flow; Condensation; Moist air; Nonequilibrium; Shock wave; Supersonic jet; Under-Expanded jet

1. Introduction

Under-expanded free jet is one of the simplest flows that have a number of practical applications ranging from the design of rocket propulsion systems to industrial areas using high pressure gas. A large number of works have been made to investigate the major features of sonic free jets [1-3]. According to these studies, the flow pattern of a jet issuing from a nozzle or an orifice depends primarily on the ratio of the pressure at the nozzle exit to the ambient pressure. Depending on this pressure ratio, three types of jets are possible: subsonic, moderately under-expanded and highly under-expanded jets. The values of pressure ratio separating these three flow patterns are dependent on the specific heat of the gas, although the variation from one gas to another gas is quite small [4, 5].

In the subsonic free jets, the pressure at the exit of nozzle is always matched with the ambient pressure, while the jet becomes underexpanded, as the pressure at the exit of nozzle is higher than the ambient pressure. With an increase in the pressure ratio at the nozzle exit to the ambient pressure, the sonic jet is changed from the moderately underexpanded to the highly underexpanded jets. These two jets are mostly distinguished by the appearance of the Mach disk inside the jet [6-8].

Many previous studies have shown that the Mach

† This paper was recommended for publication in revised form by Associate Editor Do Hyung Lee

*Corresponding author. Tel.: +82 54 820 5622, Fax.: +82 54 820 6127
E-mail address: kimhd@andong.ac.kr

© KSME & Springer 2009

disk is one of the most important factors specifying the highly underexpanded sonic jets. Billig et al., [9] Saito et al. [10] and Narayanan & Damodaran [11] have investigated the diameter of Mach disk, the distance from the exit of nozzle to the Mach disk and the configuration of the jet boundary. They have documented that all these are a function of the pressure ratio only. Addy [12] has argued that from some experimental works using several different nozzles, the nozzle configuration does not affect the distance of the Mach disk, but he has pointed out that it can somewhat influence the Mach disk diameter. Many other researchers [13, 14] have reported similar results to the work of Addy.

Cumber et al. [14] have collected the experimental data obtained by many other researchers, and showed that the distance of the Mach disk correlates quite well with the pressure ratio, but the correlation in the Mach disk diameters is relatively poor. However, they did not give detailed explanation for this poor correlation, and vaguely inferred that it could result from the difference of the nozzle geometries used in each experiment. Recently, Matsuo et al. [15] and Otobe et al. [16] have reported that the poor correlation in the Mach disk diameters is due to the vena contracta phenomenon, formed in the orifice nozzles used in various experimental works, and they have demonstrated a good correlation using an imaginary nozzle throat concept based on the vena contracta.

Meanwhile, several works have been performed to investigate the effects of the working gas on supersonic free jets. [17, 18] According to these results, the specific heat ratio of the working gas influences the jet pressure ratio as well as the convective velocities of the gas particles. The supersonic jets are often applied in power plants and industrial manufacturing processes. In these applications, the working gas is usually steam or moist air, which has not received the same level of attention in supersonic jet technologies as single-phase gases. Baek et al. [19] and Otobe et al. [20] have experimentally and numerically investigated the Mach disk phenomenon, which is formed in under-expanded most air jet, and have reported that the moist air jets are qualitatively similar with the dry air jets, but nonequilibrium condensation in the moist air jet affects the Mach disk diameter, since the nonequilibrium condensation of the moisture component changes the local flow states just upstream of the Mach disk.

As mentioned above, provided that the pressure ratio and nozzle geometry are given, the structures of under-expanded jet are well known. As the pressure ratio increases over a certain critical value, corresponding to a sonic condition at the exit of nozzle, regular reflection of shock wave occurs in the weakly under-expanded jet. Then, as the pressure increases further, the regular reflection transitions to Mach reflection, leading to the Mach disk on the jet axis. On the contrary, the Mach reflection reduces again to the regular reflection, as the jet pressure ratio decreases.

Recently, Irie et al. [21] observed that a hysteresis phenomenon of the under-expanded dry air jet is produced during the transient processes of jet pressure ratio, in which the jet flow obtained in the startup transient is different from that in the shutdown transient. In many industrial and engineering applications of under-expanded jets, the jet pressure ratio is changing during a process. However, only a few works have, to date, been devoted to the jet hysteresis, and its physical reasoning to cause the phenomenon is still not satisfactorily known. Moreover, there is no work to investigate the hysteresis phenomenon in under-expanded moist air jets, so far.

In the present study, the under-expanded moist air jets, corresponding to the range of moderately under-expanded to strongly under-expanded conditions have been investigated with the help of a computational fluid dynamics method. The jet pressure ratio is changed to obtain the hysteresis phenomenon. Quasi-steady computational analysis is carried out to numerically solve the axisymmetric, compressible Navier-Stokes equations. Initial relative humidity at the nozzle supply is assumed to get different moist air jets. The present computations are validated with the experimental data. The results obtained show that the hysteresis behavior appears in both dry and moist air jets, but the moist air jets lead to much less hysteresis, compared with the dry air jets.

2. Computational analysis

2.1 Governing equations

Computational predictions are performed by using two-dimensional, unsteady, compressible Navier-Stokes equations, which combine a nucleation rate equation and a droplet growth equation. The present computations neglect interphase velocity and temperature slip, and are given in detail by Ref.22. It is assumed that the condensation particles have a negligible effect on the pressure field. The conservation equa-

tions of mass, momentum and energy for the viscous adiabatic compressible flow of the mixture are given being similar to their single phase flow. The resulting governing equations are given in the axisymmetric coordinate system (x, y)(y : the radial distance from the axis),

$$\frac{\partial U}{\partial t}+\frac{\partial E}{\partial x}+\frac{\partial F}{\partial y}=\frac{1}{Re}\left(\frac{\partial R}{\partial x}+\frac{\partial S}{\partial y}\right)+\frac{1}{y}H+Q \tag{1}$$

where

$$\mathbf{S}=\begin{bmatrix}0\\ \tau_{yx}\\ \tau_{yy}\\ \beta\\ 0\\ 0\\ 0\\ 0\end{bmatrix},\ \mathbf{R}=\begin{bmatrix}0\\ \tau_{xx}\\ \tau_{xy}\\ \alpha\\ 0\\ 0\\ 0\\ 0\end{bmatrix},\ \mathbf{U}=\begin{bmatrix}\rho_m\\ \rho_m u\\ \rho_m v\\ E_s\\ \rho_m g\\ \rho_m D_1\\ \rho_m D_2\\ \rho_m D_3\end{bmatrix},$$

$$\mathbf{E}=\begin{bmatrix}\rho_m u\\ \rho_m u^2+p\\ \rho_m uv\\ u(E_s+p)\\ \rho_m ug\\ \rho_m uD_1\\ \rho_m uD_2\\ \rho_m uD_3\end{bmatrix},\ \mathbf{F}=\begin{bmatrix}\rho_m v\\ \rho_m uv\\ \rho_m v^2+p\\ v(E_s+p)\\ \rho_m vg\\ \rho_m vD_1\\ \rho_m vD_2\\ \rho_m vD_3\end{bmatrix},$$

$$\mathbf{H}=\begin{bmatrix}-\rho v\\ -\rho uv\\ -\rho v^2\\ -v(E_s+p)\\ -\rho gv\\ -\rho D_1 v\\ -\rho D_2 v\\ -\rho D_3 v\end{bmatrix},\ \mathbf{Q}=\begin{bmatrix}0\\ 0\\ 0\\ 0\\ \rho_m\dot{g}\\ \rho_m\dot{D}_1\\ \rho_m\dot{D}_2\\ \rho_m\dot{D}_3\end{bmatrix} \tag{2}$$

In Eq.(2), Es and p are the total energy per unit volume and the static pressure, respectively, and these are expressed by,

$$E_s=\rho_m C_{p0}T+\frac{1}{2}\rho_m\left(u^2+v^2\right)-\rho_m gL \tag{3}$$

$$p=G\left[E_s-\frac{1}{2}\rho_m\left(u^2+v^2\right)+\rho_m gL\right] \tag{4}$$

where,

$$G=\left(1-g\frac{M_m}{M_v}\right)\Big/\left(\frac{1}{\gamma-1}+g\frac{M_m}{M_v}\right) \tag{5}$$

In Eq.(2), the first component is the continuity equation, the second and third components are the Navier-Stokes equations corresponding to x and y directions, the fourth component is the energy equation, and the rate of the liquid-phase production is expressed by the equations from the fifth to eighth components. α and β are given by,

$$\alpha=u\tau_{xx}+v\tau_{yx}+k\frac{\partial T}{\partial x},\ \beta=u\tau_{xy}+v\tau_{yy}+k\frac{\partial T}{\partial y} \tag{6}$$

where τ_{xx}, τ_{xy}, τ_{yx} and τ_{yy} are components of viscous shear stresses. Subscripts *m* and *v* refer to mixture and vapor component, respectively. *k* is the thermal conductivity. The latent heat *L* is given by a function of temperature [23, 24],

$$L(T)=L_0+L_1T\ \ \text{J/kg} \tag{7}$$

where the coefficients are given by :

$$L_0=3105913.39\ \ \text{J/kg},\ \ L_1=-2212.97\ \ \text{J/kg}$$

The condensate mass fraction g is given by a rate equation, expressed by Eq. (8). [22]

$$\dot{g}=\frac{dg}{dt}=\frac{\rho_l}{\rho_m}\left(\frac{4\pi}{3}r_c^3 I+\rho_m D_1\frac{dr}{dt}\right) \tag{8}$$

In Eq.(2), $\dot{D}_1$, $\dot{D}_2$, and $\dot{D}_3$ are given as :

$$\dot{D}_1=\frac{dD_1}{dt}=\frac{4\pi r_c^2 I}{\rho_m}+D_2\frac{dr}{dt} \tag{9}$$

$$\dot{D}_2=\frac{dD_2}{dt}=\frac{8\pi r_c I}{\rho_m}+D_3\frac{dr}{dt} \tag{10}$$

$$\dot{D}_3=\frac{dD_3}{dt}=\frac{8\pi I}{\rho_m} \tag{11}$$

Nucleation rate *I*, critical radius of the nuclei r_c and radius growth rate $\dot{r}$ are given as follows [22, 23]:

$$I=\frac{1}{\rho_l}\left(\frac{2m_v\sigma}{\pi}\right)^{1/2}\left(\frac{p_v}{\kappa T}\right)\exp\left(\frac{-4\pi r_c\sigma}{3T\kappa}\right) \tag{12}$$

$$r_c=\frac{2\sigma}{\rho_l\Re_v T\ln\left(p_v/p_{s,\infty}\right)} \tag{13}$$

$$\dot{r} = \frac{dr}{dt} = \frac{1}{\rho_l}\frac{p_v - p_{s,r}}{(2\pi\Re_v T)^{1/2}} \quad (14)$$

In the above equations, m, κ, $\Re$ and $p_{s,\infty}$ are the molecular weight, Boltzmann constant, the gas constant and the flat film equilibrium vapor pressure, respectively. The density of liquid phase is given by a function of temperature [24],

$$\left.\begin{aligned}\rho_l(T) &= \frac{A_0 + A_1 t + A_2 t^2 + A_3 t^3 + A_4 t^4 + A_5 t^5}{1 + B_0 t} \\ &\quad \text{kg/m}^3, (t \geq 0\ ^\circ\text{C}) \\ \rho_l(T) &= A_6 + A_7 t + A_8 t^2 \\ &\quad \text{kg/m}^3, (t < 0\ ^\circ\text{C})\end{aligned}\right\} \quad (15)$$

where t is the temperature given by °C and the coefficients are given by,

$A_0 = 999.8396$, $A_1 = 18.224944$, $A_2 = -7.92221 \times 10^{-6}$
$A_3 = -55.44846 \times 10^{-6}$, $A_4 = -149.7562 \times 10^{-9}$
$A_5 = -393.2952 \times 10^{-12}$, $A_6 = 999.84$, $A_7 = 0.086$,
$A_8 = -0.0108$, $B_0 = 18.159725 \times 10^{-3}$

The surface tension $\sigma\ (=\sigma_\infty)$, that is an infinite flat-film surface, is given by,

$$\left.\begin{aligned}\sigma_\infty(T) &= \{76.1 + 0.155(273.15 - T)\} \times 10^{-3}, \\ &\quad \text{for } T \geq 249.39\ \text{K} \\ \sigma_\infty(T) &= \{(1.1313 - 3.7091 \times 10^{-3} \times T) \times T^4 \\ &\quad \times 10^{-4} - 5.6464\} \times 10^{-6}, \\ &\quad \text{for } T < 249.39\ \text{K}\end{aligned}\right\} \quad (16)$$

In Eq. (13), $p_{s,\infty}$ is also given as [23, 24],

$$\left.\begin{aligned}&p_{s,\infty}(T) = \\ &\exp\left(A_9 + A_{10} T + A_{11} T^2 + B_1 \ln(T) + \frac{C_0}{T}\right) \text{N/m}^3\end{aligned}\right\} \quad (17)$$

where the coefficients are given by :

$A_9 = 21.125$, $A_{10} = -2.7246 \times 10^{-2}$, $A_{11} = 1.6853 \times 10^{-5}$,
$B_1 = 2.4576$, $C_0 = -6094.4642$

where T is given by the temperature (K). Using flat film equilibrium vapor pressure $p_{s,\infty}$ above, the saturation vapor pressure $p_{s,r}$ of condensate droplet with a radius of r in Eq. (14) is given by Thompson-Gibbs equation, [23, 24]

$$p_{s,r} = p_{s,\infty} \exp\left(\frac{2\sigma_\infty}{\rho_l \Re_v T r}\right) \quad (18)$$

The governing equation systems are non-dimensionalized with the reference values at the inlet conditions upstream of the nozzle and then these are mapped from the physical plane into a computational plane of a general transform. To close the governing equations, the two equation, k-ω turbulence closure model is employed to solve turbulence stresses. A third-order TVD(total variation diminishing) finite difference scheme with MUSCL [25] is used to discretize the spatial derivatives of the governing equations and a second-order central difference scheme is applied to the viscous terms. A second-order fractional time step is employed for the time integration.

2.2 Boundary conditions

A cylindrical straight nozzle has a diameter of D_e=12.7mm. The nozzle is composed of a convergent curved entrance wall which has a radius of curvature R=D_e and the following straight wall having its length of 0.4D_e. This is exactly the same as that used by Addy [12] so that the present computational results can be validated with his data as well as the present experiments.

Moist air is assumed as the working gas, and its initial relative humidity at the nozzle supply is given by a function of the initial degree of supersaturation S_0. The jet pressure ratio of moist air is defined as φ which means the ratio of total pressure p_0 at the nozzle supply to back pressure p_b. In the present study, φ varies from 3.0 to 6.2, and the initial degree of supersaturation S_0 of moist air is changed between 0(dry air) and 0.8. The upstream total temperature T_0 and total pressure p_0 are assumed to maintain constant at 298.15K and 101.3kPa, respectively, through the whole computations.

The fixed upstream boundary conditions were applied to the upstream boundary of the computational domain, and the downstream boundary was subject to the outflow conditions. Adiabatic and no-slip boundary conditions were applied to the solid wall surfaces. Further, condensate mass fraction was assumed to be zero at the nozzle wall surfaces. According to several preliminary computations, it was known that numerical waves were propagating far upstream of the nozzle

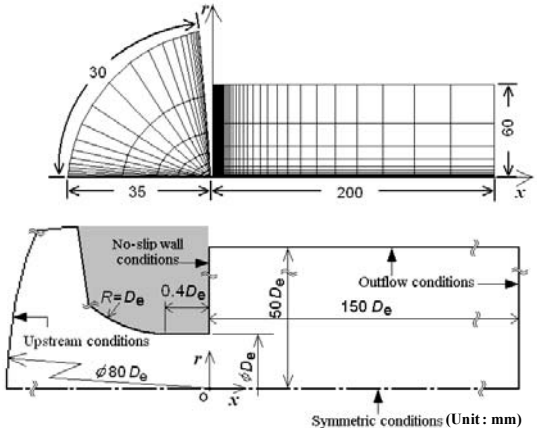

Fig. 1. Computational grid mesh and boundary conditions.

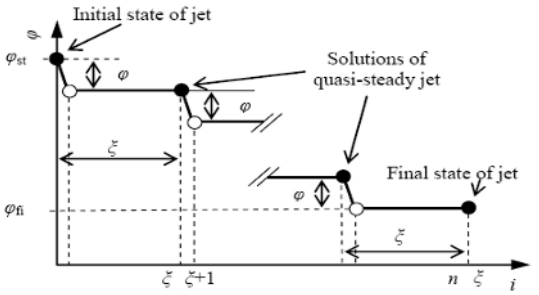

Fig. 2. Computation procedure to simulate the processes of shutdown and startup transients.

inlet. Hence, the upstream domain in the present computations extends to the distance of $80D_e$ upstream from the nozzle exit, while the downstream domain covers the region of 150 D_e and 50 D_e from the nozzle exit, in the x- and r-directions, respectively. This wide computational domain was required to ensure the computational domain independent solutions.

Fig. 1 shows a typical grid system employed in the present computations. The computational grids were clustered in the flow regions with large gradient such as the wall boundary layer, shock wave and nozzle exit. The computational grids closest to the nozzle walls are located at 0.00154 mm away from the walls. Several preliminary computations have been performed on different computational grid meshes to investigate the grid-independent solutions. According to these results, it is found that the grid meshes over 0.1 millions no longer influence the solutions obtained.

2.3 Computational procedure

The hysteresis cycle has been often reported in several flow fields due to the nonlinear nature inherent in the flow under consideration. Such flows can be computed by numerical simulations, [26] in which the flow boundary conditions are systematically changed to obtain each of the quasi-steady solutions. Fig. 2 shows the computational procedure for the process of the shutdown transient, in which the pressure ratio is decreased. The steady under-expanded jet of $\varphi=\varphi_{st}$ is computed, and the resulting solutions are used as the initial conditions for the first step of the process of the shutdown transient. In the second step, the pressure ratio is decreased by $\Delta\varphi$ and the computation is repeated until the transient process is completed, thus leading to a quasi-steady state, as indicated by the black circle. The computed quasi-steady solutions are used again as the initial conditions for the next step. Consequently, the final quasi-steady solutions are obtained for the pressure ratio of φ_{fi}. On the contrary, for the process of the startup transient, in which the pressure ratio is increased, the final quasi-steady solutions are used again as the initial conditions. For reference, in the present study, φ_{st}=6.2, φ_{fi}=3.0, $\Delta\varphi$=0.1 and ξ=20000. Through such a series of computations, the quasi-steady solutions obtained during both the startup and shutdown transients are compared to investigate the hysteric behaviors of the under-expanded moist air jets.

3. Experimental work

Experimental work has been made to validate the present computations. A simple jet facility has been fabricated to easily visualize the hysteric behaviors of the jet. A plenum chamber is placed upstream of the convergent nozzle. Room air at atmospheric conditions enters the plenum chamber and a moisture generator and a heater controls the flow conditions inside it. The test section is placed downstream of the nozzle and optical glass windows are installed on both the side walls of the test section for flow visualization. The test section is connected to a large vacuum chamber by a ball valve system. The moist air flows through the convergent nozzle into the test section, and then is sucked into the vacuum chamber. The pressures are measured in the plenum and vacuum chambers. In the experiment, the range of the pressure ratio φ is varied between 3.6 and 6.4. The initial degree of supersaturation S_0 is changed only in the range from 0.15 to 0.7.

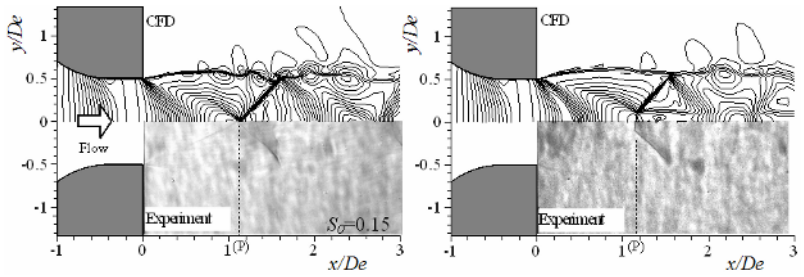

(a) S_0=0 (b) S_0=0.7

Fig. 3. Comparisons between computed and experimental results(φ=3.8).

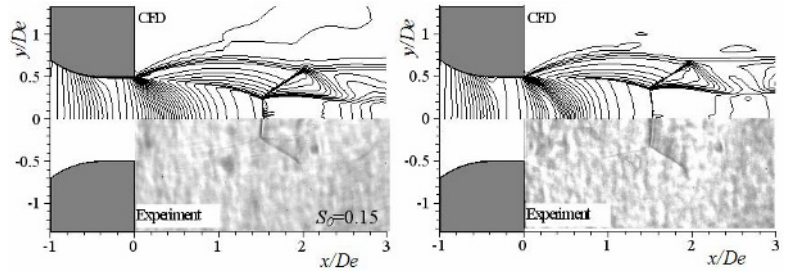

(a) S_0=0 (b) S_0=0.7

Fig. 4. Comparisons between computed and experimental results(φ=6.2).

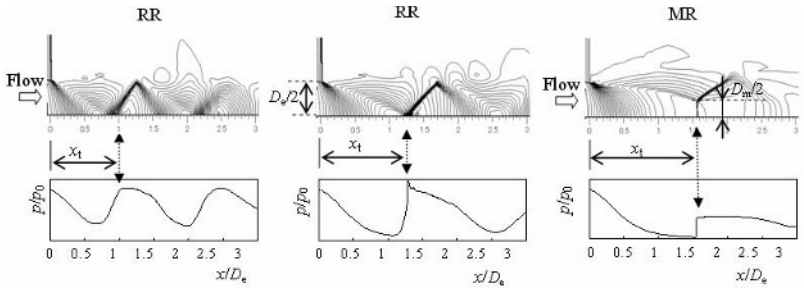

(a) φ=3.0 (b) φ=4.0 (c) φ=6.0

Fig. 5. Three flow patterns of under-expanded dry air jet (S_0=0).

4. Results and discussion

The atmospheric air as the working gas contains more or less moisture, depending on the daily weather conditions. In the present experiment, the condition of S_0=0 which corresponds to the dry air is never achieved due to limited capacity of the dehumidification system employed. The lowest value of S_0 to be reached in the experiment is at most 0.15. Thus, in the present study, the condition of S_0 =0.15 is assumed to correspond to that of the dry air in computations**.**

Figs. 3 and 4 show comparisons of the computed and experimental jets for different pressure ratio and S_0. The upper half is the computed iso-density contours and the lower half the schlieren pictures. For the dry air of S_0=0, the jet is slightly under-expanded (see Fig. 3(a)), and the resulting weak shock waves have the regular reflection at the point P. However, at S_0=0.7, the shock system becomes the Mach reflection. This difference in the two jets for the same pressure ratio is associated with the latent heat release due to the non-equilibrium condensation of moisture component. In case of φ=6.2 in Fig. 4, the dry air jet is strongly under-expanded at the nozzle exit, compared with Fig. 3(a), and thus, leads to the Mach disk on the jet axis. It is again found that the nonequilibrium condensation appreciably influences the shock structure of the dry air jet, as observed in Fig. 4; it is likely that the diame-

ter of the Mach disk grows with S0. From the comparison of the computed and experimental results it is known that the present computations predict the under-expanded dry and moist jets with good accuracy.

Fig. 5 shows three typical flow patterns of the under expanded dry air jets (S_0=0), which are obtainable depending on the pressure ratio. At φ=3.0, the jet structure is composed of a multiple of cells and the static pressure distribution along the jet axis is quite similar to a sinusoidal wave (see Fig. 5(a)). At φ=4.0, the barrel shock waves are formed, each of them intersecting on the jet axis. The resulting shock pattern is regular reflection (RR) (see Fig. 5(b)). In this case, the static pressure has a local peak value at the intersection point which is located at x_t. At φ=6.0, the Mach disk occurs at a position of x_t from the nozzle exit, leading to a sudden pressure jump. It is interesting to note that a plateau in the pressure distribution occurs just downstream of the Mach disk, unlike the two cases of φ=3.0 and 4.0. The flow is subsonic just downstream of the Mach disk, and the resulting shock pattern poses the Mach reflection (MR). It is, thus, considered that the under-expanded dry air jet systematically changes from Fig. 5(a) to Fig. 5(c), during the startup transient of jet.

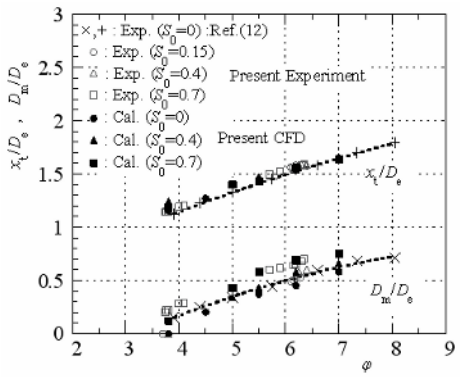

Fig. 6. The variations of x_t/D_e and D_m/D_e with φ.

Fig. 6 represents the validation of the present computations for the steady jets. The prediction results of the present computations for the under-expanded dry and moist air jets are compared with the present experimental and Addy's data. All of the predicted x_t/D_e data show that they can be given by an increasing function of the pressure ratio and are well correlated with the present experimental data as well as Addy's data. It is likely that S_0 does not significantly influence x_t/D_e. Meanwhile, the present computations predict well the Mach disk diameter (D_m/D_e). However, it seems that the diameter of the Mach disk increases with S_0 for a given pressure ratio, as reported in Ref. [19]. It is known that the present computations predict the Mach disk characteristics for both the under-expanded dry and moist air jets, with good accuracy.

Many researchers have even observed the hysteric behaviors occurring during both the startup and shut-down transients in a variety of flow fields. However, detailed reasoning and mechanisms of the hysteresis phenomenon are still not answered satisfactorily. Recently Irie et al. [21] showed that the under-expanded dry air jets behave hysteric during both the processes of the startup and shutdown transients of the jet. To investigate such a hysteresis phenomenon, the unsteady computational analysis has been performed for both the under-expanded dry and moist air jets, as previously described.

Fig. 7 shows the computed iso-density contours for

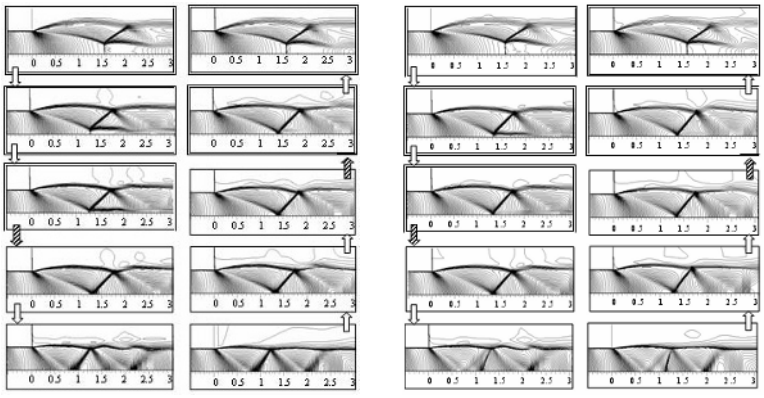

(a) S_0=0 (b) S_0=0.3

Fig. 7. The under-expanded dry and moist air jets during shut-down and startup transients.

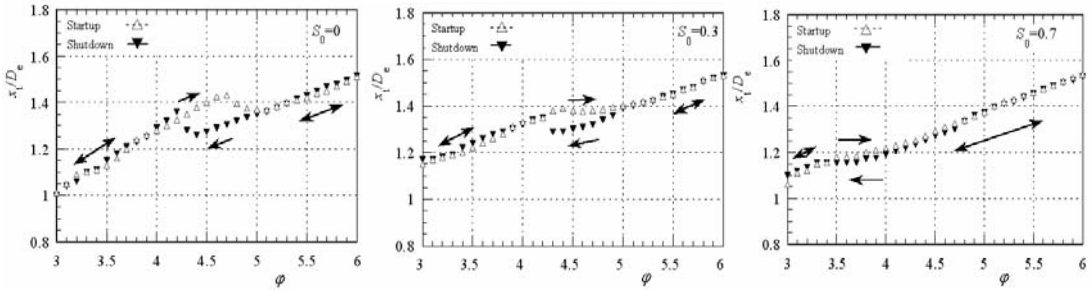

(a) S_0=0 (b) S_0=0.3 (c) S_0=0.7

Fig. 8. Hysteric behavior in the Mach disk locations during shutdown and startup transients.

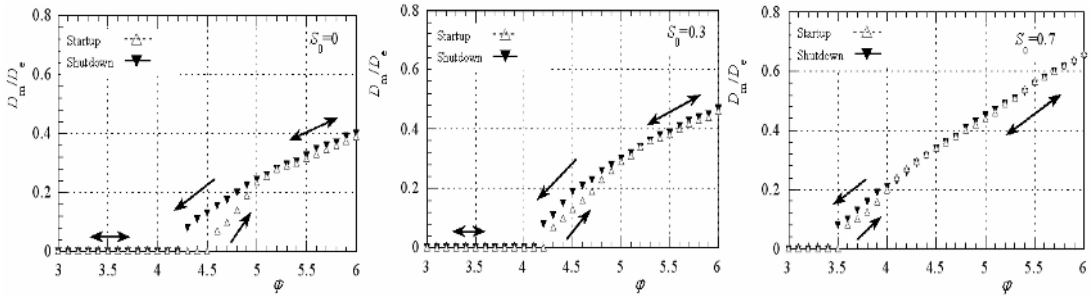

(a) S_0=0 (b) S_0=0.3 (c) S_0=0.7

Fig. 9. Hysteric behavior in the Mach disk diameters during shutdown and startup transients.

the under-expanded dry(see Fig. 7(a)) and moist air(see Fig. 7(b)) jets. For the dry air jets, the jet is strongly under-expanded at φ=6.2, the barrel shock waves reflect from the jet axis, leading to the Mach disk at the location of x_t/D_e=1.57. A triple point is formed at the intersection point among the three shocks of barrel shock, Mach disk and reflected shock, and downstream of it, the slip stream is generated due to the velocity difference in the flows passing over the two oblique shocks and the Mach disk. As φ decreases to 4.6, the Mach disk moves upstream with reduced diameter. At φ=4.2, the Mach disk is no longer found and the resulting shock pattern becomes the regular reflection. With further decrease in the pressure ratio, the shock system of the regular reflection moves upstream and its magnitude seems to be weaker. During this shutdown transient of jet, the transition from the Mach disk to the regular reflection flows appears at φ=4.2.

Meanwhile, the jet pressure ratio is increased again from the final steady jet state (φ=3.0), which has been employed in the shutdown transient above. As φ increases to 4.2, the regular reflection shocks move downstream with stronger magnitude. The transition from the regular reflection to the Mach reflection flows is generated at φ=4.55. With further increase in the pressure ratio, the Mach disk grows and its location moves downstream. At φ=6.2 which corresponds to the final steady jet state in the startup transient, the computed flow field is nearly the same to that employed as the initial conditions in the shutdown transient. From a series of computations, it is found that the pressure ratio at which the transition occurs is significantly different in both the processes of the shutdown and startup transients. Similar hysteric behavior is also found in the under-expanded moist air jets, as shown in Fig.7(b), where the transition pressure ratio occurs at φ=4.15 in the shutdown transient but at 4.25 in the startup transient. It is, however, noted that the hysteresis phenomenon appears to be reduced in the moist air jet, compared with the dry air jet.

More quantitative data for the hysteresis phenomena are presented in Fig.8, where the locations of the shock reflection during both processes in the shutdown and startup transients are plotted against the het pressure ratio. For the dry air het (see Fig.8(a)), in the process of the startup transient, the shock reflection point moves downstream with an increase in φ, and it has a peak at φ=4.55, which corresponds to the transition pressure ratio. As φ increases over transition pressure ratio, the shock reflection point moves a little upstream, and then it moves downstream again with

further increase in φ. On the contrary, in the process on the shutdown transient, the shock reflection point moves upstream with a decrease in φ, and it has a peak at φ=4.25 corresponding to the transition pressure ratio. Then it moves again upstream with further decrease in φ. A hysteric loop in the shock reflection point is found in both the transient processes. It seems that the hysteresis loop is reduced in the moist air jets(see Fig. 8(b) and 8(c)).

Fig. 9 shows the hysteric behavior in the diameter of the Mach disk. For the dry air jets, it is found that in the process of the startup transient, the incipient Mach disk occurs at φ =4.5 and its diameter increases with an increase in φ . On the contrary, in the process of the shutdown transient, it decreases with φ . At φ =4.25, the Mach reflection flow transitions to the regular reflection, leading to D_m/D_e =0.0. Therefore, the hysteric behavior is produced during both the processes of the shutdown and startup transients. It seems that such a hysteresis phenomenon in the diameter of the Mach disk is reduced in the moist air jets(see Fig. 9(b) and (c)). It is interesting to note that the pressure ratio for the incipient Mach disk decreases with S_0. This is due to the nonequilibrium condensation which occurs depending on a local supersaturation of the flow. Inside the jets, the condensation of moisture component causes the deceleration of local flow due to the latent heat release [27]. This modifies the local structure of jet, leading to the incipient Mach disk at lower pressure ratio, compared with the dry air jets.

Fig. 10 presents the effect of nonequilibrium condensation on the static pressure distributions during both the processes of the shutdown and startup transients. It is noted that for the dry air jet, the static pressure distribution along the jet axis is the same as an isentrope as schematically shown in Fig. 10(a), but for the moist air jet it deviates from the isentrope due to the latent heat release of nonequilibrium condensation. The resulting difference between these two distributions would be an effect of nonequilibrium condensation that occurs during both the processes of the shutdown and startup transients. For reference, Fig. 10(b) represents the deviation in both the static pressure distributions for S0=0.3 and the startup transient. It is also noted that the Mach reflection is produced for φ =4.6 and 5.0 cases, while the regular reflection is obtained for the cases less than φ =4.2. In the Mach reflection flows, the deviation is not big, but appears over a wide range of x/De. However, in the regular reflection flows, it is relatively big, but occurs in a narrow region.

For both the processes of the shutdown and startup transients, the variation of the static pressures just upstream and downstream of shock wave is plotted in Fig. 11, where the results of steady jet computations are denoted by symbol ×. The symbols and ▲ are the static pressures just upstream of shock wave, respectively, for the regular reflection and Mach reflection in the transient processes, while the symbols ○ and ● are the static pressures just downstream of shock wave, respectively, for the regular reflection and Mach reflection. For the startup transient, regular reflection occurs in the range less than φ =4.55, while Mach reflection higher than φ =4.55. However, this boundary is changed to φ =4.25 in the process of shutdown transient. It is known that the static pressure jump of the regular reflection is much higher than that of the Mach reflection. The transition from regular to Mach reflections is generated as the static pressure jump due to shock wave is the highest. The difference between the quasi steady and steady jets becomes appreciable mainly near the pressure ratio that the transition occurs.

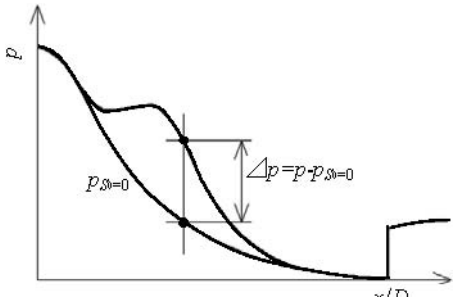

(a) Schematic diagram of ⊿p

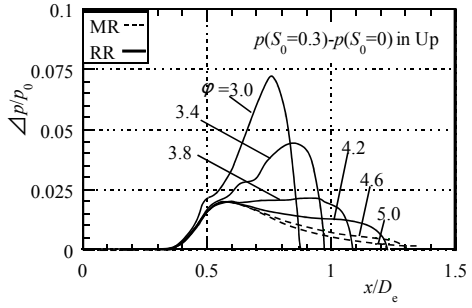

(b) P distribution

Fig. 10. Difference between the static pressure distributions of dry and moist air jets.

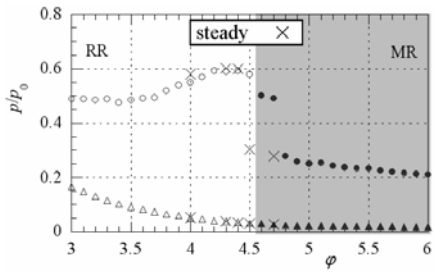

(a) Startup transient

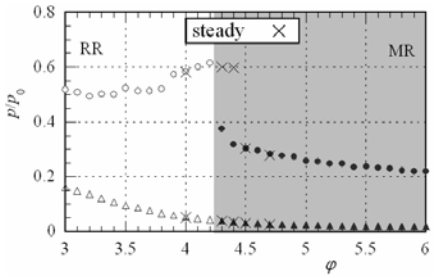

(b) Shutdown transient

Fig. 11. Variations in the static pressures just upstream and downstream of shock wave(S_0=0).

5. Concluding remarks

The present study deals with the computational and experimental works to investigate under-expanded dry and moist air jets. The two-dimensional, unsteady, compressible Navier-Stokes equations have been used to numerically solve the flow field concerning with the hysteric behavior in both the processes of the shutdown and startup transients of the jet. A nucleation rate equation and a droplet growth equation are combined with the governing equation system to simulate nonequilibrium condensation of moisture component in the under-expanded moist air jets. The present computations predict well the major features of the dry and moist air jets as well as the hysteric behaviors occurring in the shutdown and startup transients of jet. The results obtained show that the hysteric phenomenon is produced both in the under-expanded dry air and moist air jets. Such hysteresis effects are given in terms of the locations and diameters in the Mach disk, and they are reduced with the initial degree of supersaturation of moist air at the nozzle supply. This means that the under-expanded moist air jet leads to less hysteresis of the jet, compared with the dry air jets. It is known that non-equilibrium condensation, which occurs in the under-expanded moist air jet, is responsible for these findings.

References

[1] S. G. Chuech, M. C. Lai and G. M. Faeth, Structure of turbulent sonic underexpanded free jets, *AIAA Journal*, 27 (1989) 549-559.

[2] S. G. E. A. Meier, W. C. Selerowicz and A. P. Szumowski, A nozzle generating low jet noise, *Journal of Sound and Vibration* , 136 (1990) 65-73.

[3] P. Birkby and G. J. Page, Numerical predictions of turbulent underexpanded sonic jets using a pressure-based methodology, *IMechE*, 215 (2001) 165-173.

[4] R. T. Driftmyer, A correlation of freejet data, *AIAA Journal*, 10 (1972) 1093-1095.

[5] J. L. Palmer and R. K. Hanson, Application of method of characteristics to underexpanded, freejet flows with vibrational nonequilibrium, *AIAA Journal*, 36 (1998) 193-200.

[6] JR. T. C. Adamson and J. A. Nicholls, On the structure of jets from highly underexpanded nozzle into still air, *Journal of the Aero/Space Sciences*, January (1959) 16-24.

[7] H. Ashkenas and F. S. Sherman, The structure and utilization of supersonic free jets in low density wind tunnels, *Rarefied Gas Dynamics*, 2 (1966) 84-105.

[8] A. Powell, The sound-producing oscillations of round underexpanded jets impinging on normal plates, *J. Acoust. Soc. Am.*, 83 (1988) 515-533.

[9] F. S. Billig, R. C. Orth and M. Lasky, A unified analysis of gaseous jet penetration, *AIAA Journal*, 9 (1971) 1048-1058.

[10] T. Saito, H. Nakatsuji and K. Teshima, Numerical simulation and visualization of freejet flow-fields, *Trans. Japanese Soc. Aero. Space Sci*., 28 (1986) 240-247.

[11] A. K. Narayanan and K. A. Damodaran, Mach disk of dual coaxial axisymmetric jets. *AIAA Journal*, 31 (1993) 1343-1345.

[12] A. L. Addy, Effects of axisymetric sonic nozzle geometry on mach disk characteristics, *AIAA Journal,* 19 (1981) 121-122.

[13] J. C. Lengrand, J. Allegre and M. Raffin, Underexpanded free jets and interaction with adjacent surfaces. *AIAA Journal*, 20 (1982) 27-28.

[14] P. S. Cumber, M. Fairweather, S. A. E. G. Falle and J. R. Giddings, Predictions of the structure of turbulent, highly underexpanded jets, *Trans. ASME, Journal of Fluids Engineering*, 117 (1995) 599-604.

[15] S. Matsuo, M. Tanaka, Y. Otobe, H. Kashimura,

H.-D. Kim and T. Setoguchi, Effect of axisymmetric sonic nozzle geometry on characteristics of supersonic air jet, *Journal of Thermal Science*, 13 (2004) 121-126.

[16] Y. Otobe, H. Kashimura, S. Matsuo, T. Setoguchi and H.-D. Kim, Influence of nozzle geometry on the near-field structure of a highly underexpanded sonic jet, *Journal of Fluids and Structures*, 24 (2008) 281-293.

[17] C. H. Lewis and Jr, D. J. Carlson, Normal shock location in underexpanded gas and gas-particle jets, *AIAA Journal*, 2 (1964) 776-777.

[18] A. B. Bauer, Normal shock location in underexpanded gas-particle jets, *AIAA Journal*, 3 (1965) 1187-1189.

[19] S.-C. Baek, S.-B. Kwon, H.-D. Kim, T. Setoguchi and S. Matsuo, Study of moderately underexpanded supersonic moist air jets, *AIAA Journal*, 44 (2006) 1624-1627.

[20] Y. Otobe, S. Matsuo, M. Tanaka, H. Kashimura and T. Setoguchi, A study on characteristics of under-expanded condensing jet, *JSME International Journal, Series B*, 49 (2006) 1165-1172.

[21] T. Irie, T. Yasunobu, H. Kashimura and T. Setoguchi, Hysteresis phenomena of mach disk formation in an underexpanded jet, *Theoretical and Applied Mechanics Japan*, 53 (2004) 181-187.

[22] S. Matsuo, Y. Otobe, M. Tanaka, H. Kashimura, T. Setoguchi and S. Yu, Effect of non-equilibrium condensation on axisymmetric under-expanded jet, *International Journal of Turbo and Jet Engines*, 21 (2004) 193-201.

[23] G. H. Schnerr, Homogene kondensation in stationären transsonischen strömungen durch laval-dusen und um profile, Habilitationsschrift, Universität Karlsruhe(TH), Germany, (1986).

[24] S. Adam, Numerische und experimentelle untersuchung instationarer dusenstromungen mit energiezufuhr durch homogene kondensation, Dissertation, Fukaltat fur Maschinenbau, Universitat Karlsruhe (TH), Germany (1999).

[25] H. C. Yee, A class of high-resolution explicit and implicit shock capturing methods, *NASA* (1989) TM-101088.

[26] A. Nebbache and C. Pilinski, Pulsatory phenomenon in a thrust optimized contour nozzle. *Aerospace Science and Technology*, 10 (2006) 295-308.

[27] W. Frank, Condensation phenomena in supersonic nozzles, *Acta Mechanica*, 54 (1985) 135-156.

Heuy-Dong Kim received his B.S. and M.S. degrees in Mechanical Engineering from Kyungpook National University, Korea, in 1986 and 1988, respectively. He then received his Ph.D. degree from Kyushu University, Japan, in 1991. Dr. Kim is currently a Professor at the School of Mechanical Engineering, Andong National University, Korea. His research interests include High-Speed Trains, Ramiet and Scramiet, Shock Tube and Technology, Shock Wave Dynamics, Explosions & Blast Waves, Flow Measurement, Aerodynamic Noises and Supersonic Wind Tunnels.

Min-Sung Kang received his B.S. and M.S degrees in Mechanical Engineering from Andong National University, Korea, in 2007 and 2009, respectively. Mr. Kang is currently a researcher at the School of Mechanical Engineering at Andong National University, Korea. His research interests include cavity and supersonic nozzle flows.

Yumiko Otobe received her B.S. degree in Faculty of Engineering from Yamaguchi University, Japan, in 1978. She then received her Eng. D. degree from Saga University, Japan, in 2007. Dr. Otobe is currently a Research Associate at the Department of Control & Information Systems Engineering, Kitakyushu National College of Technology, Japan. Dr. Otobe's research interests include sonic and supersonic jets of various gases as well as non-equilibrium condensation phenomena.

Toshiaki Setoguchi received his B.S. degree in Mechanical Engineering from Tokyo University of Agriculture and Technology, Japan, in 1976. He then received his M.S. and Ph.D. degrees from Kyushu University, Japan, in 1978 and 1981, respectively. Dr. Setoguchi is currently a Professor at the Department of Mechanical Engineering, Saga University, Japan. His research interests include Nonequilibrium Condensation, Ramiet and Scramiet, Shock Tube and Technology, Shock Wave Dynamics, Explosions & Blast Waves, Aerodynamic Noises and Turbomachinery.